Imbalanced superfluid state in an annular disk



2009 J. Phys.: Condens. Matter 21 355701

(http://iopscience.iop.org/0953-8984/21/35/355701)

J. Phys.: Condens. Matter **21** (2009) 355701 (8pp) doi:10.1088/0953-8984/21/35/355701

# Imbalanced superfluid state in an annular disk

**Fei Ye[1,2], Yan Chen[3], Z D Wang[2] and F C Zhang[2]**

[1] Center for Advanced Study, Tsinghua University, Beijing 100084, People's Republic of China
[2] Department of Physics and Center for Theoretical and Computational Physics, The University of Hong Kong, Hong Kong, People's Republic of China
[3] Department of Physics and Lab of Advanced Materials, Fudan University, Shanghai 200433, People's Republic of China

E-mail: feiye@mail.tsinghua.edu.cn, yanchen99@fudan.edu.cn, zwang@hkucc.hku.hk and fuchun@hkucc.hku.hk

Received 29 April 2009, in final form 8 July 2009
Published 10 August 2009
Online at stacks.iop.org/JPhysCM/21/355701

**Abstract**

The imbalanced superfluid state of spin-1/2 fermions with s-wave pairing is numerically studied by solving the Bogoliubov–de Gennes equation at zero temperature in an annular disk geometry with narrow radial width. Two distinct types of systems are considered. The first case may be relevant to heavy fermion superconductors, where magnetic field causes spin imbalance via Zeeman interaction and the system is studied in a grand canonical ensemble. As the magnetic field increases, the system is transformed from the uniform superfluid state to the Fulde–Ferrell–Larkin–Ovchinnikov state, and finally to the spin polarized normal state. The second case may be relevant to cold fermionic systems, where the number of fermions of each species is fixed as in a canonical ensemble. In this case, the ground state depends on the pairing strength. For weak pairing, the order parameter exhibits a periodic domain wall lattice pattern with a localized spin distribution at low spin imbalance, and a sinusoidally modulated pattern with extended spin distribution at high spin imbalance. For strong pairing, the phase separation between the superfluid state and polarized normal state is found to be preferable, while the increase of spin imbalance simply changes the ratio between them.

(Some figures in this article are in colour only in the electronic version)

## 1. Introduction

In conventional Bardeen–Cooper–Schrieffer (BCS) theory, the normal state has a Fermi surface common to both spin-up and spin-down electrons and the Cooper pair has zero total momentum. More than 40 years ago, Fulde and Ferrell (FF) [1] and Larkin and Ovchinnikov (LO) [2] independently proposed the pairing mechanism for the mismatched Fermi surfaces due to the spin imbalance. In the FF state, a spin-up electron with momentum $\vec{k}$ is bounded with a spin-down electron with momentum $-\vec{k}+\vec{q}$; thereby the Cooper pair has a net momentum $\vec{q}$ which is determined by the imbalance between two Fermi surfaces. Therefore the order parameter is characterized by a single momentum $\vec{q}$, which can be written as $\Delta(\vec{r}) = \Delta_0 e^{i\vec{q}\cdot\vec{r}}$ with a uniform magnitude $\Delta_0$. If considering the composition of two momenta, $\vec{q}$ and $-\vec{q}$, one gets the LO state where the order parameter is real with its magnitude oscillating periodically in space.

In condensed matter physics, the spin imbalance can be generated by applied magnetic fields. However, the condition for the FFLO state to be observed is quite stringent on the superconducting materials. Roughly speaking, there are three requirements: (i) low $T_c$, so that the magnetic field needed to imbalance the spin population is accessible; (ii) the orbital effect of the magnetic field is weak enough to avoid pair breaking before the Zeeman splitting takes effect; (iii) a clean limit, i.e. the mean free path of an electron should be much longer than the correlation length, since the FFLO state is easily destroyed by impurities. Some heavy fermion superconductors are good candidates to fulfill these requirements (for a review see [3]). There have been recent indications that $CeCoIn_5$ indeed exhibits the FFLO

 

state [4–9]. That compound is a quasi-two-dimensional heavy fermion superconductor with a d-wave pairing. In the cold fermionic atom system with different hyperfine spins, the spin population imbalance between different hyperfine spins can be easily controlled by applying a radio frequency field. Recently the imbalanced superfluid state has been realized in these cold neutral atom systems [10–14], and the possible spatially modulated superfluid phases in these systems have been studied in [15, 16]. It is noted that the particle number of different species may be controlled directly in systems like cold atoms, and in superconductors the spin imbalance is generated by the external magnetic fields, which may correspond to two different thermodynamic conditions.

In a recent theoretical study [17] it was found that in the harmonically trapped polarized fermionic atoms in a two-dimensional (2D) optical lattice the insulating core is surrounded by a superfluid shell at high atomic densities with the pairing parameter modulated in the circumferential direction. Since some of the important physics may be explained by the quasi-one-dimensional (quasi-1D) shell, it is thus interesting to study the FFLO further in more detail in a quasi-1D system. The possible angular FFLO state in a toroidal trap has also been investigated in a very recent study [18]. In the present paper, we consider a quasi-1D annular disk with narrow enough radial width so that the radial modulation of the order parameter might result in quite a large radial gradient of order parameter which increases the system energy considerably according to the Ginzburg–Landau (GL) theory. Therefore the oscillation of pairing amplitude is suppressed in a radial direction, and restricted only in the circumferential direction. In a large 2D system, the order parameter oscillation has more freedom and can occur in arbitrary directions. In the presence of inhomogeneity the modulation direction may vary in space, which leads to an irregular pattern of the order parameter. Therefore it may be easier to observe regular oscillations of the pairing amplitude in a quasi-1D system than in the 2D film.

In this paper we consider two distinct systems. The first one may be relevant to heavy fermion superconductors, where the electron spins interact with an external magnetic field via the Zeeman coupling. The second system may be related to cold fermionic atoms, where the number of fermions of each spin is fixed. We employ a grand canonical ensemble to study the first system and a canonical ensemble to study the second system. We solve the Bogoliubov–de Gennes (BdG) equation numerically at zero temperature for the above quasi-1D systems. Our main results are summarized below. In the first case, as the magnetic field increases, the ground state is transformed from a uniform superfluid state to the sinusoidally modulated LO state, and then to a spin polarized normal state. In the second case, the ground state depends on the pairing strength. For weak interactions, the order parameter exhibits a periodic domain wall lattice pattern with a localized spin distribution for low spin imbalance, and a sinusoidally modulated pattern with extended spin distribution for high spin imbalance. For strong interactions, the phase separation between the superfluid state and the polarized normal state is found to be more preferable, while increase in spin imbalance simply extends the spatial region of the normal state. The paper is organized as follows. In section 2, we study the exact 1D case. In section 3, we present our results for annular disk geometry. The conclusion is given in section 4.

## 2. Imbalanced superfluid state in a one-dimensional ring

### 2.1. One-dimensional BdG equation

Before exploring the properties of an imbalanced superfluid in the annular disk geometry, we first consider a 1D ring, which may be viewed as the limiting case where the disk width is so narrow that only one radial mode is relevant. This case has been studied by a number of authors. In the mean field (MF) level, a rigorous analysis for the 1D BdG equation is given in [19] in the presence of a magnetic field. In terms of 1D Luttinger liquid theory the imbalanced superconducting state is also elucidated by Yang [20], and very recently the density matrix renormalization group algorithms have been implemented in the 1D negative-$U$ Hubbard model to explore the FFLO state in [21–24]. The cold fermionic gases with attractive interaction and population imbalance are studied theoretically in [25] and [26].

In this subsection, we follow the MF treatment to give a brief description of the 1D imbalanced superfluid state. We consider a canonical ensemble and fix the number of fermions of different species. Although only quasi-long range order may exist in a 1D system, the MF approach presented in this section is helpful to understand the imbalanced superfluid in 2D annular disk geometry shown in later sections.

The mean field Hamiltonian for a 1D interacting system reads

$$\begin{aligned}\hat{H} = &\int \mathrm{d}x \left[ \sum_{\alpha} \hat{\psi}_{\alpha}^{\dagger}(x) \left( -\frac{\hbar^2 \partial_x^2}{2m} \right) \hat{\psi}_{\alpha}(x) \right. \\ &\left. + \left( \Delta(x) \hat{\psi}_{\uparrow}^{\dagger}(x) \hat{\psi}_{\downarrow}^{\dagger}(x) + \text{h.c.} \right) - \frac{|\Delta(x)|^2}{g} \right] \\ &- \sum_{\alpha} \mu_{\alpha} \left[ \int \mathrm{d}x \hat{\psi}_{\alpha}^{\dagger}(x) \hat{\psi}_{\alpha}(x) - N_{\alpha} \right] \\ &\Delta(x) = g \left\langle \hat{\psi}_{\downarrow}(x) \hat{\psi}_{\uparrow}(x) \right\rangle . \end{aligned} \tag{1}$$

$\hat{\psi}_{\alpha}(x)$ is the fermion annihilation field at position $x$ with spin index $\alpha$, $\Delta(x)$ is the fermion pairing field, $m$ is the mass of the particle, and $g < 0$ is the attractive interaction strength. $\mu_{\alpha}$ are the Lagrangian multipliers or the chemical potentials, which are used to fix the number of fermions of different spins at $N_{\uparrow}$ and $N_{\downarrow}$, respectively.

Equation (1) has a similar form to the well known Su–Schrieffer–Heeger (SSH) model [27] for polyacetylene, which describes a 1D electron system coupled to phonons. In this system, when the phonon fields are condensed in opposite phases at the two ends of the 1D string, there are possible soliton excitations with zero energy in the fermion spectrum. The soliton excitations are also possible in the 1D superfluid Hamiltonian equation (1), where the MF pairing parameter $\Delta(x)$ can mimic the phonon field in the SSH model, which is shown briefly below. More details can be found in [19]

for example. For simplicity we take $\mu_\uparrow = \mu_\downarrow = \mu$, which determines the Fermi momentum $k_\mathrm{F} = \sqrt{2m\mu}/\hbar$. The low energy physics is described by quasiparticles around the two Fermi points $\pm k_\mathrm{F}$, i.e. the following decomposition is allowed:

$$\hat{\psi}_\sigma(x) \sim \mathrm{e}^{\mathrm{i}k_\mathrm{F}x}\hat{R}_\sigma(x) + \mathrm{e}^{-\mathrm{i}k_\mathrm{F}x}\hat{L}_\sigma(x) \tag{2}$$

with left and right movers defined as

$$\begin{aligned}\hat{R}_\sigma(x) &= \sum_{-\Lambda<k<\Lambda}\hat{\psi}_\sigma(k+k_\mathrm{F})\frac{\mathrm{e}^{\mathrm{i}kx}}{\sqrt{L}}\\ \hat{L}_\sigma(x) &= \sum_{-\Lambda<k<\Lambda}\hat{\psi}_\sigma(k-k_\mathrm{F})\frac{\mathrm{e}^{\mathrm{i}kx}}{\sqrt{L}}.\end{aligned} \tag{3}$$

$\Lambda$ is a suitable momentum cutoff. These quasiparticle operators satisfy the standard anti-commutation relations, i.e.

$$\{\hat{R}_\sigma, \hat{R}^\dagger_{\sigma'}\} = \{\hat{L}_\sigma, \hat{L}^\dagger_{\sigma'}\} = \delta_{\sigma,\sigma'}$$

and all the other anti-commutators are zero. Substituting equation (2) into equation (1), and neglecting the fast oscillation terms ($\propto \exp(\pm 2\mathrm{i}k_\mathrm{F}x)$), one obtains the following two Hamiltonians to the linear order of $k$:

$$\begin{aligned}\hat{H}_1 &= \hbar v_\mathrm{F}\int \mathrm{d}x :\hat{R}^\dagger_\uparrow(-\mathrm{i}\partial_x)\hat{R}_\uparrow: - :\hat{L}^\dagger_\downarrow(-\mathrm{i}\partial_x)\hat{L}_\downarrow:\\ &\quad + \int \mathrm{d}x\,\Delta(x)(\hat{R}^\dagger_\uparrow\hat{L}^\dagger_\downarrow + \hat{L}_\downarrow\hat{R}_\uparrow)\\ \hat{H}_2 &= \hbar v_\mathrm{F}\int \mathrm{d}x :\hat{R}^\dagger_\downarrow(-\mathrm{i}\partial_x)\hat{R}_\downarrow: - :\hat{L}^\dagger_\uparrow(-\mathrm{i}\partial_x)\hat{L}_\uparrow:\\ &\quad + \int \mathrm{d}x\,\Delta(x)(\hat{L}^\dagger_\uparrow\hat{R}^\dagger_\downarrow + \hat{R}_\downarrow\hat{L}_\uparrow).\end{aligned} \tag{4}$$

Here $:A:$ denotes normal ordering of $A$ and $v_\mathrm{F}$ means the positive Fermi velocity. In the following $\hbar v_\mathrm{F}$ is taken as unity. $\hat{H}_1$ and $\hat{H}_2$ are commutative with each other, and are connected through the gap equation

$$\Delta(x) = g\left\langle R_\downarrow L_\uparrow + L_\downarrow R_\uparrow\right\rangle. \tag{5}$$

The order parameter $\Delta(x)$ is assumed to be real. Equation (5) shows that the pairing takes place either between $\hat{L}_\uparrow$ and $\hat{R}_\downarrow$, or between $\hat{L}_\downarrow$ and $\hat{R}_\uparrow$. Actually, $\langle R_\downarrow L_\uparrow\rangle = \langle L_\downarrow R_\uparrow\rangle$ by symmetry. Formally, one may have $\hat{H} \sim \hat{H}_1 + \hat{H}_2 - \int \mathrm{d}x|\Delta(x)|^2/g$, but it is emphasized that $\hat{H}_{1,2}$ only describes the low energy excitations near the Fermi surface.

Let us consider only $H_1$ with a twisted $\Delta(x)$, i.e. $\Delta(-\infty) = -\Delta(\infty) = \Delta_0$. As shown by Jackiw and Rebbi [28], there is at least one zero mode $\hat{\gamma}_{0\uparrow}$ in the middle of the gap, which is localized in space and reads

$$\begin{aligned}\hat{\gamma}_{0\uparrow} &\propto \int \mathrm{d}x\,F(x)[\hat{R}_\uparrow(x) - \mathrm{i}\hat{L}^\dagger_\downarrow(x)]\\ F(x) &\propto \exp\left[\int_0^x \mathrm{d}x'\Delta(x')\right].\end{aligned} \tag{6}$$

It is easy to verify the commutation relation $[\hat{\gamma}_{0\uparrow}, \hat{H}_1] = 0$. Besides this localized zero mode, we also have other quasiparticle excitations $\hat{\gamma}_{n\alpha}$ in the continuum region, where $n$ and $\alpha$ are the energy level and spin indices, respectively. Assuming all of them constitute a complete representation of the Hamiltonian $H_1$, the lowest energy states are doubly degenerate in the presence of an order parameter with a kink pattern, which is the spinless vacuum of the quasiparticles $\hat{\gamma}_{n\alpha}$ together with the zero mode $\hat{\gamma}_{0\uparrow}$ being either filled or empty. Similar analysis is also valid for the $H_2$ branch, for which one can find that the zero mode has the form

$$\hat{\gamma}_{0\downarrow} \propto \int \mathrm{d}x\,F(x)[\hat{R}_\downarrow(x) + \mathrm{i}\hat{L}^\dagger_\uparrow(x)]$$

which satisfies $[\gamma_{0\downarrow}, H_2] = 0$.

In terms of $\hat{R}_\sigma$ and $\hat{L}_\sigma$, the total particle number $\hat{N}$ and total spin operator $\hat{S}$ can be written as

$$\hat{N} = \hat{N}_\uparrow + \hat{N}_\downarrow, \qquad \hat{S} = \hat{N}_\uparrow - \hat{N}_\downarrow$$

$$\hat{N}_\sigma = \int \mathrm{d}x[:\hat{R}^\dagger_\sigma\hat{R}_\sigma: + :\hat{L}^\dagger_\sigma\hat{L}_\sigma:],$$

where the fast oscillating terms are neglected. Note that the quasiparticle operators $\hat{R}_\sigma$ and $\hat{L}_\sigma$ can only describe the low energy physics, hence the operator $\hat{N}_\sigma$ with normal ordering only measures the particle number relative to the Fermi surface. Obviously, unlike the SSH model [27] and the Jackiw–Rebbi model [28], the charge conservation is broken in the BCS theory, and therefore one cannot tell how many charges the soliton can carry. Despite this fact, the total spin is still a conserved quantity in our MF treatment, therefore each zero mode may carry a half spin as an analogue to the half charge investigated in [27, 28]. But in practice only one spin can be observed at the kink of $\Delta(x)$, since there are two branches of fermions ($H_1$ and $H_2$). To observe the half spin, one must get rid of the fermion doubling problem. Nevertheless, this provides a mechanism to accommodate excess spins with zero energy. The total energy of the soliton measured relative to the uniform BCS state is computed to be $2\Delta_0/\pi$ [29, 30], which is less than the superfluid gap.

### *2.2. From soliton lattice-like LO state to sinusoidally varying LO state*

For equally populated species $N_\uparrow = N_\downarrow$, the lowest energy state is obviously the BCS state with a uniform pairing gap. If one spin is flipped from downward to upward, i.e. $N_\uparrow + 1$ up spin and $N_\downarrow - 1$ down spin, a soliton–anti-soliton pair is developed to store these two excess spins. We define the spin imbalance $n$ to be $(N_\uparrow - N_\downarrow)/2$ for spin 1/2 particle. A typical soliton–anti-soliton pair is plotted in figure 1(a), which is obtained by numerically solving equation (1) in a ring, where we use the angle $\theta = 2\pi x/L$ as the coordinate. Due to the periodic boundary condition, a single soliton cannot exist freely so that it must co-exist with an anti-soliton as a pair with the same width $\xi$. We call these soliton states with each spin per soliton (anti-soliton) an *ideal soliton* state. Note that since the order parameter is real, this state is also a kind of LO state. Actually, all the self-consistent solutions shown in this paper have real order parameters which minimize the energy, and therefore they are LO states. In the following sections, we omit 'LO' for the sake of brevity.

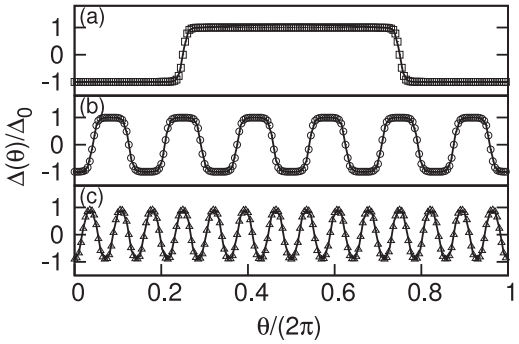


**Figure 1.** Angle distribution of the pairing order parameter in an ideal soliton state. The order parameter is measured in units of $\Delta_0$ which is the value of order parameter in the uniform state. From top to bottom, total spin imbalance is 1, 6 and 14. Open symbols: numerical results; solid lines: fitting function $\tilde{\Delta}\tanh(\cos n\theta/\tilde{\xi})$ with two parameters $\tilde{\Delta}$ and $\tilde{\xi}$.

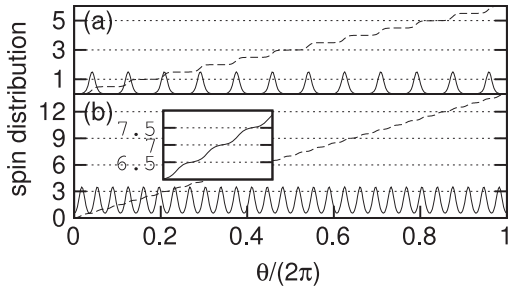


**Figure 2.** Spin distribution in the soliton lattice state for the system with spin imbalance 6 (a) and 14 (b). Solid lines: local spin distribution; dashed lines: integrated spin distribution. The inset of (b) shows a zoomed figure around a plateau.

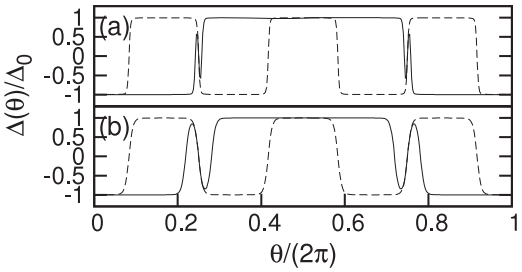


**Figure 3.** Pairing parameter in a deformed soliton with $\mathcal{Q} = 3$ (solid lines) and an ideal soliton with $\mathcal{Q} = 1$ (dashed lines). The upper (lower) panel corresponds to the strong (weak) pairing interaction $g$.

With the increase of the flipped spins, more soliton–anti-soliton pairs are generated. Thus we get the *soliton lattice* state with $n$ pairs of solitons and anti-solitons as long as the system is in the *dilute limit* by which we mean $n\xi \ll 2\pi$, here the soliton width $\xi$ is measured in unit of the angle. In the dilute limit, the solitons are well separated from each other, which has two consequences: (i) all the midgap states have zero energy; and (ii) each soliton or anti-soliton carries exactly one localized spin. According to these two properties, we distinguish the soliton lattice state from the sinusoidally modulated state, where the spin imbalance $n$ is too large to satisfy $n\xi < 2\pi$ and solitons overlap considerably with each other. Then the energy spectrum of the midgap states has a dispersion described by the Bloch theorem for a periodic lattice. Such a scenario from soliton lattice to sinusoidally varying state has also been addressed in [31] from the viewpoint of GL theory. The pairing parameter for both states can be described perfectly by the fitting function[4] $\tilde{\Delta}\tanh(\cos n\theta/\tilde{\xi})$ with $\tilde{\Delta}$ and $\tilde{\xi}$ to be determined, which is shown in figure 1.

We now introduce two spin distribution functions, local spin distribution $S_L(\theta) = \frac{1}{2}\langle\hat{\psi}^\dagger_\uparrow(\theta)\hat{\psi}_\uparrow(\theta) - \hat{\psi}^\dagger_\downarrow(\theta)\hat{\psi}_\downarrow(\theta)\rangle$ as well as integrated spin distribution $S_I(\theta)$,

$$S_I(\theta) = \int_0^\theta S_L(\theta')\,\mathrm{d}\theta'. \tag{7}$$

As shown in figure 2, the localization of spin density in the soliton lattice state manifests itself in the plateau features of the function $S_I(\theta)$. For the sinusoidally modulated state, the plateaus disappear due to the delocalization of spins.

### 2.3. Deformed soliton

Here we introduce $\mathcal{Q}$ to denote the number of spins per soliton/anti-soliton. In the previous subsections, we focused on the state with only one spin ($\mathcal{Q} = 1$) per soliton. Now we study the case for $\mathcal{Q} \geqslant 2$, which we call the *deformed soliton* state. Firstly, let us consider the case for odd $\mathcal{Q}$. The order parameter of a deformed soliton state for $\mathcal{Q} = 3$ is plotted in figure 3 (solid lines), which corresponds to six excess spins in total. Note that these six spins can also be stored in three ideal soliton–anti-soliton pairs (dashed lines). Hence, we need to compare their energies numerically. It turns out that the deformed soliton is energetically favorable for strong interaction, while the ideal soliton state is preferable for weak interaction. Note that the deformed soliton found in this article has $\mathcal{Q}$ nodes in a narrow region. In fact $\mathcal{Q}$ spins can also be accommodated by a special soliton with only one node, which is described by $\Delta_0\tanh(x/\xi)$ with $\Delta_0\xi = (\mathcal{Q}+1)/2$ (see [30]); however one can show that this solution is not energetically favored by comparing its energy and that of the corresponding well separated multi-soliton state.

In figure 3, the upper panel corresponds to a strong interaction case where the three spins are squeezed in a very narrow region with width comparable to that of an ideal soliton $\xi$. The total width is then estimated to be around $2\xi$, which is much smaller than the width $6\xi$ for the ideal soliton state. Thus, one can reasonably believe that the deformed soliton state has lower energy. If the interaction strength $g$ becomes weaker, as shown in the lower panel of figure 3, the deformed soliton with $\mathcal{Q} = 3$ will inflate and its pattern gets close to three ideal solitons. When $g$ becomes weak enough, the deformed soliton cannot be stable, and is transmuted into an ideal soliton lattice state. The pairing order parameter shown in figure 3 can be perfectly fitted with the function $\tilde{\Delta}_0[\tanh(\cos(\theta-\theta_0)/\tilde{\xi}_0) - \tanh(\cos(\theta)/\tilde{\xi}_0 + \tanh(\cos(\theta+\theta_0)/\tilde{\xi}_0]$ with three parameters $\tilde{\Delta}_0$, $\tilde{\xi}_0$ and $\tilde{\theta}_0$.

[4] The soliton lattice pattern of pairing parameters can be described by the Jacobi elliptic function as done in [19], but we do not include that expression for the sake of simplicity.

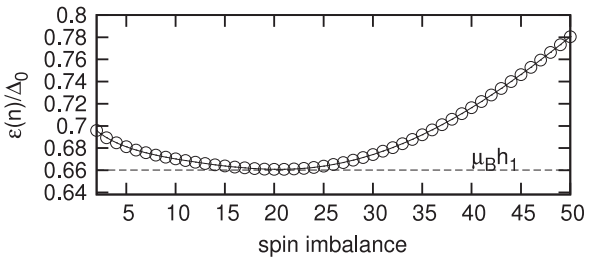


**Figure 4.** Average energy per spin $\varepsilon(n)$ in equation (8) as a function of spin imbalance $n$. The dashed line is the first critical magnetic field $h_1$.

Note that the order parameter has a sign change $(-1)^{\mathcal{Q}}$ after crossing $\mathcal{Q}$ ideal solitons and anti-solitons. Therefore, if $\mathcal{Q}$ is odd, a deformed soliton can be continuously transmuted into $\mathcal{Q}$ ideal solitons, but this is not true for even $\mathcal{Q}$ due to the mismatched boundary condition of $\Delta(x)$. In addition, the energy of a deformed soliton with even $\mathcal{Q}$ is not energetically favorable in our numerical calculations. Therefore, we do not need to consider the case for even $\mathcal{Q}$.

### *2.4. Effect of a magnetic field*

So far we have only considered the system with fixed particle number, and have not included the magnetic field in our analysis. Since the total spin is a good quantum number, the effect of magnetic field can be easily estimated by simply adding Zeeman energy $-\mu_B h(N_\uparrow - N_\downarrow)$. Obviously, the state with more excess spins gains magnetic energy; however, it is at the cost of the deformation of pairing gap which loses the condensation energy. Therefore, the ground state should correspond to an optimized value of spin imbalance.

Let $n = (N_\uparrow - N_\downarrow)/2$ be the spin imbalance, and the corresponding ground state energy be denoted by $E(n)$. The energy of the BCS state without spin imbalance is thus $E(0)$. Given an external magnetic field $h$, we then need to find the lowest free energy for all possible $n$ s, i.e. minimize $E(n) - 2n\mu_B h$ with respect to $n$, which leads to an optimal spin imbalance $n_c$.

To this end we define the energy cost per spin as

$$\varepsilon(n) \equiv [E(n) - E(0)]/(2n), \tag{8}$$

which can also be regarded as the energy cost for creating one soliton. The numerical data for $\varepsilon(n)$ are plotted in figure 4. As $n$ increases, the adjacent kinks become closer, which enhances the hopping amplitude of spins between kinks and consequently favors the kinetic energy of spin transfer. However, at the same time, the pairing gap gets smaller, which reduces the condensation energy. Thus the interplay between these two mechanisms leads to the nontrivial pattern of $\varepsilon(n)$ in figure 4.

There is a critical value $h_1$ of the magnetic field below which the magnetic energy cannot support an ideal soliton, and the system remains in the uniform state. When $h > h_1$, the sinusoidally varying state with modulation frequency $n_c$ will become energetically favorable. $n_c$ can be determined by the minimum of $2n\varepsilon(n) - 2n\mu_B h$; alternatively, the optimal spin imbalance $n_c$ should satisfy

$$\left.\frac{\partial(2n(\epsilon(n) - \mu_B h))}{\partial n}\right|_{n=n_c} = 0. \tag{9}$$

After a little algebraic analysis of equation (9), one can see that $n_c$ increases as $h$ increases. The first $n_c$ is determined by $\epsilon(n_c) = \mu_B h_1$ which is far from zero as shown in figure 4 and corresponds to a sinusoidally modulated state.

## 3. Imbalanced superfluid state in annular disk

In this section we present our numerical results for an imbalanced superfluid state in narrow annular disk with inner radius $R_1$ and outer radius $R_2$. The radial width $R_2 - R_1$ is small enough to avoid the modulation of order parameter along the radial direction. In the numerical calculation, we use the ratio $\rho \equiv (R_2 - R_1)/R_1$ to characterize the geometry of an annular disk. Since $g$ has the dimension of [energy] $\cdot$ [length]$^2$, a dimensionless quantity $\tilde{g} \equiv g/(\pi(R_2^2 - R_1^2)\mu)$ is introduced to represent the interaction strength. The BdG equation is solved in momentum space. Most of the results in this section are based upon the diagonalization of a Hamiltonian in a Hilbert space with dimensionality 3500 and 11 radial modes involved.

### *3.1. Fixing particle number $N_\uparrow$ and $N_\downarrow$*

*3.1.1. An ideal domain wall.* For small spin imbalance, one should get domain walls as an analog of solitons in the 1D case, and the excess spins are attached to the domain walls. It is natural to ask what is the optimal number ($\mathcal{Q}$) of spins per domain wall? To answer this question, we first consider an ideal geometry, i.e. a narrow strip with periodic boundary conditions in both $x$ and $y$ directions, but with length $L_x \gg L_y$.

This simplified model reads

$$\begin{aligned}\hat{H} = \int \mathrm{d}x\,\mathrm{d}y \Bigg[ & \hat{\psi}_\alpha^\dagger \left(\frac{\hat{\vec{p}}^2}{2m} - \mu_\alpha\right)\hat{\psi}_\alpha \\ & + \Delta(x,y)\hat{\psi}_\uparrow^\dagger\hat{\psi}_\downarrow^\dagger + \Delta^*(x,y)\hat{\psi}_\downarrow\hat{\psi}_\uparrow - \frac{|\Delta(x,y)|^2}{g}\Bigg] \\ \Delta(x,y) = & \, g\left\langle\hat{\psi}_\downarrow\hat{\psi}_\uparrow\right\rangle.\end{aligned} \tag{10}$$

The ideal domain wall pattern of $\Delta(x,y)$ is independent of $y$, and has the form $\Delta(x,y) = \Delta_0 \tanh(x/\xi_0)$, which implies that the pairing momenta in the $y$ direction are always $q$ and $-q$. The Hamiltonian in equation (10) can be divided into many 1D branches with respect to the discrete momenta $q = (2\pi/L_y) \times$ integer in the $y$ direction:

$$\begin{aligned}\hat{H}_q \sim \int \mathrm{d}x \Bigg[ & \hat{\psi}_{q,\uparrow}^\dagger(x)\left(\frac{\hat{p}_x^2}{2m} - \mu_{q\uparrow}\right)\hat{\psi}_{q,\uparrow}(x) \\ & + \hat{\psi}_{-q,\downarrow}^\dagger(x)\left(\frac{\hat{p}_x^2}{2m} - \mu_{-q\downarrow}\right)\hat{\psi}_{-q,\downarrow}(x) \\ & + \Delta\hat{\psi}_{q,\uparrow}^\dagger(x)\hat{\psi}_{-q,\downarrow}^\dagger(x) + \Delta^*\hat{\psi}_{-q,\downarrow}(x)\hat{\psi}_{q,\uparrow}(x)\Bigg].\end{aligned} \tag{11}$$

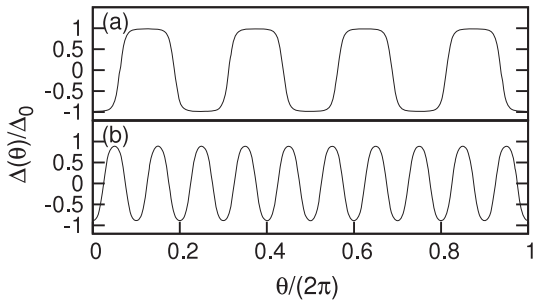


**Figure 5.** Angle dependence of the pairing order parameter at radius $(R_1 + R_2)/2$: (a) domain wall lattice state with total spin 28; (b) sinusoidally varying LO state with total spin 70. The optimal filling per domain wall is $\mathcal{Q} = 7$. The system parameter $\rho = 0.4$.

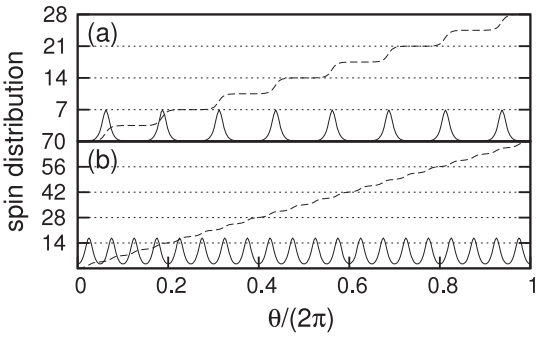


**Figure 6.** Spin distribution in the domain wall lattice state with spin imbalance 28 (upper panel) and in the sinusoidally varying state with spin imbalance 70 (lower panel). Dashed lines, integrated spin distribution $S_I(\theta)$; solid lines, local spin distribution $S_L(\theta)$. The system parameters are the same as in figure 5.

Note that all 1D branches contribute to $\Delta(x)$, and the $q$-dependent chemical potential reads $\mu_{q\alpha} = \mu_\alpha - (\hbar q)^2/(2m)$, which are determined by the particle numbers $N_\alpha$. Each $q$-mode with $\mu_q > 0$ can accommodate one spin per soliton. Therefore, we can estimate the optimal spin filling $\mathcal{Q}$ of each ideal domain wall to be the number of $q$-modes buried under the FS. The optimal filling for the annular disk with open boundary conditions in the radial direction can also be estimated similarly by counting the number of energy modes under the FS.

Similar to the 1D ring, one expects a crossover from an ideal domain wall like LO state to the sinusoidally varying LO state with increasing spin imbalance in the weak interaction case. Since $\Delta(r, \theta)$ now depends on $r$, we plot the angle dependence of $\Delta(r, \theta)$ at radius $r = (R_1 + R_2)/2$ in figure 5. The full spatial dependence of $\Delta(r, \theta)$ is plotted in 2D contours in figure 7, where one can find that its radial dependence is nearly uniform. The spin density $s(r, \theta)$ is also a function of $r$ and $\theta$. By integrating $s(r, \theta)$ over $r$, we can define angle dependent local spin distribution $S_L(\theta)$ and angle dependent integrated spin distribution $S_I(\theta)$ as follows:

$$S_L(\theta) = \int_{R_1}^{R_2} r\, \mathrm{d}r s(r, \theta)$$
$$S_I(\theta) = \int_0^{\theta} S_L(\theta)\, \mathrm{d}\theta'. \tag{12}$$

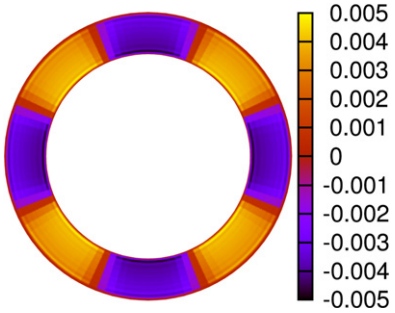


**Figure 7.** Contour plot of the order parameter. The excess spin equals 28 and the optimal filling in this case is $\mathcal{Q} = 7$, hence four pairs of domain walls are needed to store these excess spins. The system parameters are the same as in figure 5.

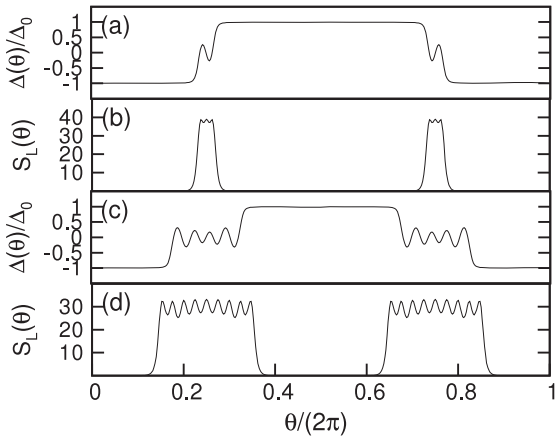


**Figure 8.** Deformed domain wall ((a) and (b)) and phase separation ((c) and (d)) solutions. We plot the order parameter in (a) and (c), and spin distribution in (b) and (d). The spin imbalance is 21 for (a) and (b) and 77 for (c) and (d). The optimal spin filling $\mathcal{Q} = 7$. The interaction strength is $\tilde{g} \sim 6.9 \times 10^{-4}$.

$S_L$ and $S_I$ are plotted as functions of $\theta$ in figure 6, which shows clearly that the spin distributions are localized in the domain wall state and delocalized in the sinusoidally varying LO state.

*3.1.2. Deformed domain wall and phase separation.* As in the 1D ring, we also encounter the deformed domain wall state, for which there can be more spins than the optimal filling $\mathcal{Q}$ squeezed in one domain wall. These deformed domain wall states are stabilized by the *strong* pairing interaction. We plot the order parameter $\Delta(\theta, r)$ and local spin distribution $S_L(\theta)$ in figure 8, which shows that when the spin number exceeds the optimal filling, instead of creating more ideal domain walls, the spin polarized regions are simply enlarged. Note that in the polarized region there is still a small pairing oscillation like a mini sinusoidally varying LO state in order to further lower the potential energy. These deformed domain wall states (see figure 8(c)) are then considered as a kind of *phase separation* state, where the polarized normal state with small fluctuating order parameter is separated with the fully pairing phase without spin imbalance.

*3.1.3. Quasiparticle density of states.* We compute the quasiparticle density of states (DOS) in this section which

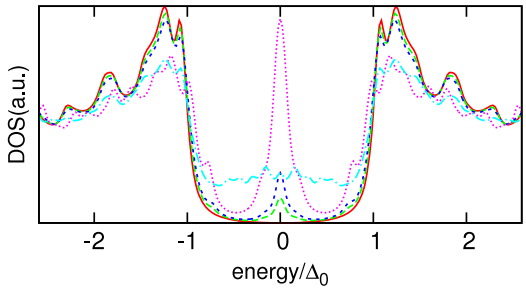


**Figure 9.** Quasiparticle density of states for different ground states. The Zeeman energy is not included in this figure. The red solid line is for the uniform BCS state, the green long dashed line and the blue short dashed line are for the domain wall lattice states, the dotted pink line is for the sinusoidally modulated LO state, and the cyan dot-dashed line corresponds to the phase separation state.

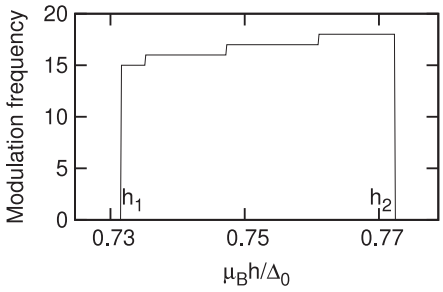


**Figure 10.** Frequency of pairing modulation as a function of magnetic field. We set $\rho = 0.2$, and $\tilde{g} = 5 \times 10^{-4}$. $\mu_B$ is the Bohr magneton, and the $g$-factor of an electron is taken as 2.

can describe the low energy excitations of various ground states. In our calculation the Zeeman energy is not included, which corresponds to the situation with fixed particle numbers. We find that for the domain wall lattice state there is a zero energy peak in the quasiparticle DOS. As the spin imbalance is increasing, the number of domain walls grows and it results in enhancement of the zero energy peak. These zero modes can also be understood from the aspect of Andreev reflection [32], since the $\pi$-phase difference between two superfluids permits an Andreev bound state located at the domain walls. In the phase separation case, the system mimics a superconductor–normal metal–superconductor junction. By increasing the width of the normal metal region, more Andreev resonance states enter into the gap with nonzero energy. These energy levels then distribute evenly in the gap, which forms a flat quasiparticle DOS in the superconducting gap.

The above theoretical analysis is in good agreement with the numerical results presented in figure 9. The DOS of the BCS state is zero in the gap. When increasing the spin imbalance in the ideal domain wall lattice state, the peak of the DOS centered around zero becomes higher, which means more domain walls are created, whereas in the case of phase separation the DOS in the gap is quite flat due to the presence of polarized normal state.

### *3.2. Fixing chemical potentials $\mu_\uparrow$ and $\mu_\downarrow$*

In this subsection, we show the numerical results in the grand canonical ensemble with fixed chemical potentials. For a weak magnetic field ($2\mu_B h = \mu_\uparrow - \mu_\downarrow$), the Zeeman energy is not enough to break the s-wave Cooper pairs, so the system retains the uniform BCS state. Until the magnetic field $h$ exceeds its first critical value $h_1$, the sinusoidally varying LO state emerges. As the magnetic field is further increased, the modulation frequency of the order parameter becomes larger while its magnitude is reduced, until the system enters into the normal state at the second critical magnetic field $h_2$. We plot modulation frequency as a function of $h$ in figure 10, where one can find plateaus since there should be integral pairs of domain walls in a ring geometry.

The phase separation (deformed domain wall) state cannot be a ground state in the homogeneous magnetic field, except at the critical value $h_1$ of magnetic field. Furthermore, unlike the case of fixed particle number, there is no continuous crossover from the domain wall state to the sinusoidally varying state. The onset frequency at the critical magnetic field $h_1$ is finite and large enough to form a sinusoidally varying LO state. The reason is that, to sustain a single domain wall, its magnetic energy gain must fully compensate the energy loss due to the deformation of the pairing gap. In such a case there can be more domain walls. However, the overlap of domain walls inevitably suppresses the pairing gap, which causes loss of the condensate energy (see section 2.4). At the balance point of these two processes, a sinusoidally varying state appears accompanied with delocalized spins.

## 4. Conclusion

We have investigated the imbalanced superfluid state in annular disks and 1D rings by solving the BdG equation in momentum space at zero temperature. A key issue with an imbalanced superfluid is how to accommodate the excess spins by adjusting the pairing gap $\Delta(\vec{r})$. There are several possibilities, e.g. the LO state with periodically oscillated order parameter and the phase separation state. We show that these states are stable under different conditions.

Firstly, we have studied the case with fixed fermion numbers, which may be relevant to cold atom systems. For low spin imbalance (still larger than the optimal spin filling $\mathcal{Q}$ per domain wall), the solitons in 1D and domain walls in 2D are the ground states. The number of spins localized at each soliton or domain wall is quantized. With increasing spin imbalance, more and more domain walls (solitons) occur and overlap with each other, and the sinusoidally varying state emerges with delocalized spins. These two states are distinguished in this paper due to their different spin distributions. There should be a crossover between them if one tunes the spin imbalance continuously. The above argument is valid for weak interactions, whereas for strong interactions the phase separation is the possible ground state, in which only the area of the normal polarized state varies with the spin imbalance. This may serve as a criterion to distinguish the phase separation state and the periodically oscillating LO state.

Secondly, we have addressed the case of fixing the chemical potential $\mu$ and magnetic field $h$, which may be relevant to heavy fermion superconductors interacting with an

external magnetic field via the Zeeman term. There are two critical magnetic fields $h_1$ and $h_2$, which correspond to the transition from a uniform BCS state to the sinusoidally varying state, and from the sinusoidally varying state to the normal state, respectively. It is stressed that the modulation frequency of the pairing gap at $h_1$ is quite large and the spin is delocalized, which characterizes a typical sinusoidally varying state.

## Acknowledgments

FY would like to thank T Li, H Zhai and Z B Su for many stimulating discussions. This work was supported by RGC grants in HKSAR, the National Natural Science Foundation of China (grants 1054700 and 10874032) and the State Key Programs of China (grant no. 2009CB929204). YC acknowledges the program for Professor of Special Appointment (Eastern Scholar) at Shanghai Institutions of Higher Learning and Shanghai Municipal Government.

## References

[1] Fulde P and Ferrell R A 1964 *Phys. Rev.* **135** A550
[2] Larkin A I and Ovchinnikov Yu N 1965 *Sov. Phys.—JETP* **20** 762
[3] Matsuda Y and Shimahara H 2007 *J. Phys. Soc. Japan* **76** 051005
[4] Radovan H A, Fortune N A, Murphy T P, Hannahs S T, Palm E C, Tozer S W and Hall D 2003 *Nature* **425** 51
[5] Bianchi A, Movshovich R, Capan C, Pagliuso P G and Sarrao J L 2003 *Phys. Rev. Lett.* **91** 187004
[6] Capan C, Bianchi A, Movshovich R, Christianson A D, Malinowski A, Hundley M F, Lacerda A, Pagliuso P G and Sarrao J L 2004 *Phys. Rev.* B **70** 134513
[7] Watanabe T, Kasahara Y, Izawa K, Sakakibara T, Matsuda Y, van der Beek C J, Hanaguri T, Shishido H, Settai R and Onuki Y 2004 *Phys. Rev.* B **70** 020506(R)
[8] Miclea C F, Nicklas M, Parker D, Maki K, Sarrao J L, Thompson J D, Sparn G and Steglich F 2006 *Phys. Rev. Lett.* **96** 117001
[9] Kumagai K, Saitoh M, Oyaizu T, Furukawa Y, Takashima S, Nohara M, Takagi H and Matsuda Y 2006 *Phys. Rev. Lett.* **97** 227002
[10] Zwierlein M W, Schirotzek A, Schunck C H and Ketterle W 2006 *Science* **311** 492
[11] Zwierlein M W, Schunck C H, Schirotzek A and Ketterle W 2006 *Nature* **442** 54
[12] Partridge G B, Li W, Kamar R I, Liao Y A and Hulet R G 2006 *Science* **311** 503
[13] Partridge G B, Li W, Liao Y A, Hulet R G, Haque M and Stoof H T C 2006 *Phys. Rev. Lett.* **97** 190407
[14] Shin Y, Zwierlein M W, Schunck C W, Schirotzek A and Ketterle W 2006 *Phys. Rev. Lett.* **97** 030401
[15] Mizushima T, Machida K and Ichioka M 2005 *Phys. Rev. Lett.* **94** 060404
[16] Machida K, Mizushima T and Ichioka M 2006 *Phys. Rev. Lett.* **97** 120407
[17] Chen Y, Wang Z D, Zhang F C and Ting C S 2009 *Phys. Rev.* B **79** 054512
[18] Yanase Y 2009 arXiv:0902.2275v1 [cond-mat]
[19] Machida K and Nakanishi H 1984 *Phys. Rev.* B **30** 122
[20] Yang K 2001 *Phys. Rev.* B **63** 140511(R)
[21] Feiguin A E and Heidrich-Meisner F 2007 *Phys. Rev.* B **76** 220508(R)
[22] Rizzi M, Polini M, Cazalilla M A, Bakhtiari M R, Tosi M P and Fazio R 2008 *Phys. Rev.* B **77** 245105
[23] Tezuka M and Ueda M 2008 *Phys. Rev. Lett.* **100** 110403
[24] Feiguin A E and Heidrich-Meisner F 2009 *Phys. Rev. Lett.* **102** 076403
[25] Orso G 2007 *Phys. Rev. Lett.* **98** 070402
[26] Hu H, Liu X-J and Drummond P D 2007 *Phys. Rev. Lett.* **98** 070403
[27] Su W P, Schrieffer J R and Heeger A J 1979 *Phys. Rev. Lett.* **42** 1698
[28] Jackiw R and Rebbi C 1976 *Phys. Rev.* D **13** 3398
[29] Dashen R F, Hasslacher B and Neveu A 1975 *Phys. Rev.* D **12** 2443
[30] Takayama H, Lin-Liu Y R and Maki K 1980 *Phys. Rev.* B **21** 2388
[31] Buzdin A I and Kachkachi H 1997 *Phys. Lett.* A **225** 341
[32] Vorontsov A B, Sauls J A and Graf M J 2005 *Phys. Rev.* B **72** 184501